P H Y S I C A L   R E V I E W   L E T T E R S

Indications of Conical Emission of Charged Hadrons at the BNL Relativistic Heavy Ion Collider

B. I. Abelev,[9] M. M. Aggarwal,[30] Z. Ahammed,[46] B. D. Anderson,[19] D. Arkhipkin,[13] G. S. Averichev,[12] Y. Bai,[28]
J. Balewski,[23] O. Barannikova,[9] L. S. Barnby,[2] J. Baudot,[17] S. Baumgart,[51] D. R. Beavis,[3] R. Bellwied,[49] F. Benedosso,[28]
R. R. Betts,[9] S. Bhardwaj,[35] A. Bhasin,[18] A. K. Bhati,[30] H. Bichsel,[48] J. Bielcik,[11] J. Bielcikova,[11] B. Biritz,[6] L. C. Bland,[3]
M. Bombara,[2] B. E. Bonner,[36] M. Botje,[28] J. Bouchet,[19] E. Braidot,[28] A. V. Brandin,[26] E. Bruna,[51] S. Bueltmann,[3]
T. P. Burton,[2] M. Bystersky,[11] X. Z. Cai,[39] H. Caines,[51] M. Calderón de la Barca Sánchez,[5] J. Callner,[9] O. Catu,[51]
D. Cebra,[5] R. Cendejas,[6] M. C. Cervantes,[41] Z. Chajecki,[29] P. Chaloupka,[11] S. Chattopadhyay,[46] H. F. Chen,[38] J. H. Chen,[39]
J. Y. Chen,[50] J. Cheng,[43] M. Cherney,[10] A. Chikanian,[51] K. E. Choi,[34] W. Christie,[3] S. U. Chung,[3] R. F. Clarke,[41]
M. J. M. Codrington,[41] J. P. Coffin,[17] T. M. Cormier,[49] M. R. Cosentino,[37] J. G. Cramer,[48] H. J. Crawford,[4] D. Das,[5]
S. Dash,[14] M. Daugherity,[42] C. De Silva,[49] M. M. de Moura,[37] T. G. Dedovich,[12] M. DePhillips,[3] A. A. Derevschikov,[32]
R. Derradi de Souza,[7] L. Didenko,[3] P. Djawotho,[16] S. M. Dogra,[18] X. Dong,[22] J. L. Drachenberg,[41] J. E. Draper,[5] F. Du,[51]
J. C. Dunlop,[3] M. R. Dutta Mazumdar,[46] W. R. Edwards,[22] L. G. Efimov,[12] E. Elhalhuli,[2] M. Elnimr,[49] V. Emelianov,[26]
J. Engelage,[4] G. Eppley,[36] B. Erazmus,[40] M. Estienne,[17] L. Eun,[31] P. Fachini,[3] R. Fatemi,[20] J. Fedorisin,[12] A. Feng,[50]
P. Filip,[13] E. Finch,[51] V. Fine,[3] Y. Fisyak,[3] C. A. Gagliardi,[41] L. Gaillard,[2] D. R. Gangadharan,[6] M. S. Ganti,[46]
E. Garcia-Solis,[9] V. Ghazikhanian,[6] P. Ghosh,[46] Y. N. Gorbunov,[10] A. Gordon,[3] O. Grebenyuk,[22] D. Grosnick,[45]
B. Grube,[34] S. M. Guertin,[6] K. S. F. F. Guimaraes,[37] A. Gupta,[18] N. Gupta,[18] W. Guryn,[3] B. Haag,[5] T. J. Hallman,[3]
A. Hamed,[41] J. W. Harris,[51] W. He,[16] M. Heinz,[51] S. Heppelmann,[31] B. Hippolyte,[17] A. Hirsch,[33] E. Hjort,[22]
A. M. Hoffman,[23] G. W. Hoffmann,[42] D. J. Hofman,[9] R. S. Hollis,[9] H. Z. Huang,[6] T. J. Humanic,[29] G. Igo,[6] A. Iordanova,[9]
P. Jacobs,[22] W. W. Jacobs,[16] P. Jakl,[11] F. Jin,[39] P. G. Jones,[2] E. G. Judd,[4] S. Kabana,[40] K. Kajimoto,[42]
K. Kang,[43] J. Kapitan,[11] M. Kaplan,[8] D. Keane,[19] A. Kechechyan,[12] D. Kettler,[48] V. Yu. Khodyrev,[32] J. Kiryluk,[22]
A. Kisiel,[29] S. R. Klein,[22] A. G. Knospe,[51] A. Kocoloski,[23] D. D. Koetke,[45] M. Kopytine,[19] L. Kotchenda,[26] V. Kouchpil,[11]
P. Kravtsov,[26] V. I. Kravtsov,[32] K. Krueger,[1] M. Krus,[11] C. Kuhn,[17] L. Kumar,[30] P. Kurnadi,[6] M. A. C. Lamont,[3]
J. M. Landgraf,[3] S. LaPointe,[49] J. Lauret,[3] A. Lebedev,[3] R. Lednicky,[13] C-H. Lee,[34] M. J. LeVine,[3] C. Li,[38] Y. Li,[43]
G. Lin,[51] X. Lin,[50] S. J. Lindenbaum,[27] M. A. Lisa,[29] F. Liu,[50] H. Liu,[5] J. Liu,[36] L. Liu,[50] T. Ljubicic,[3] W. J. Llope,[36]
R. S. Longacre,[3] W. A. Love,[3] Y. Lu,[38] T. Ludlam,[3] D. Lynn,[3] G. L. Ma,[39] Y. G. Ma,[39] D. P. Mahapatra,[14] R. Majka,[51]
O. I. Mall,[5] L. K. Mangotra,[18] R. Manweiler,[45] S. Margetis,[19] C. Markert,[42] H. S. Matis,[22] Yu. A. Matulenko,[32]
T. S. McShane,[10] A. Meschanin,[32] J. Millane,[23] M. L. Miller,[23] N. G. Minaev,[32] S. Mioduszewski,[41] A. Mischke,[28]
J. Mitchell,[36] B. Mohanty,[46] L. Molnar,[33] D. A. Morozov,[32] M. G. Munhoz,[37] B. K. Nandi,[15] C. Nattrass,[51] T. K. Nayak,[46]
J. M. Nelson,[2] C. Nepali,[19] P. K. Netrakanti,[33] M. J. Ng,[4] L. V. Nogach,[32] S. B. Nurushev,[32] G. Odyniec,[22] A. Ogawa,[3]
H. Okada,[3] V. Okorokov,[26] D. Olson,[22] M. Pachr,[11] B. S. Page,[16] S. K. Pal,[46] Y. Pandit,[19] Y. Panebratsev,[12] T. Pawlak,[47]
T. Peitzmann,[28] V. Perevoztchikov,[3] C. Perkins,[4] W. Peryt,[47] S. C. Phatak,[14] M. Planinic,[52] J. Pluta,[47] N. Poljak,[52]
A. M. Poskanzer,[22] B. V. K. S. Potukuchi,[18] D. Prindle,[48] C. Pruneau,[49] N. K. Pruthi,[30] J. Putschke,[51] R. Raniwala,[35]
S. Raniwala,[35] R. L. Ray,[42] R. Reed,[5] A. Ridiger,[26] H. G. Ritter,[22] J. B. Roberts,[36] O. V. Rogachevskiy,[12] J. L. Romero,[5]
A. Rose,[22] C. Roy,[40] L. Ruan,[3] M. J. Russcher,[28] V. Rykov,[19] R. Sahoo,[40] I. Sakrejda,[22] T. Sakuma,[23] S. Salur,[22]
J. Sandweiss,[51] M. Sarsour,[41] J. Schambach,[42] R. P. Scharenberg,[33] N. Schmitz,[24] J. Seger,[10] I. Selyuzhenkov,[16]
P. Seyboth,[24] A. Shabetai,[17] E. Shahaliev,[12] M. Shao,[38] M. Sharma,[49] S. S. Shi,[50] X-H. Shi,[39] E. P. Sichtermann,[22]
F. Simon,[24] R. N. Singaraju,[46] M. J. Skoby,[33] N. Smirnov,[51] R. Snellings,[28] P. Sorensen,[3] J. Sowinski,[16] H. M. Spinka,[1]
B. Srivastava,[33] A. Stadnik,[12] T. D. S. Stanislaus,[45] D. Staszak,[6] M. Strikhanov,[26] B. Stringfellow,[33] A. A. P. Suaide,[37]
M. C. Suarez,[9] N. L. Subba,[19] M. Sumbera,[11] X. M. Sun,[22] Y. Sun,[38] Z. Sun,[21] B. Surrow,[23] T. J. M. Symons,[22]
A. Szanto de Toledo,[37] J. Takahashi,[7] A. H. Tang,[3] Z. Tang,[38] T. Tarnowsky,[33] D. Thein,[42] J. H. Thomas,[22] J. Tian,[39]
A. R. Timmins,[2] S. Timoshenko,[26] D. Tlusty,[11] M. Tokarev,[12] T. A. Trainor,[48] V. N. Tram,[22] A. L. Trattner,[4]
S. Trentalange,[6] R. E. Tribble,[41] O. D. Tsai,[6] J. Ulery,[33] T. Ullrich,[3] D. G. Underwood,[1] G. Van Buren,[3] M. van Leeuwen,[28]
A. M. Vander Molen,[25] J. A. Vanfossen, Jr.,[19] R. Varma,[15] G. M. S. Vasconcelos,[7] I. M. Vasilevski,[13] A. N. Vasiliev,[32]
F. Videbaek,[3] S. E. Vigdor,[16] Y. P. Viyogi,[14] S. Vokal,[12] S. A. Voloshin,[49] M. Wada,[42] W. T. Waggoner,[10] F. Wang,[33]
G. Wang,[6] J. S. Wang,[21] Q. Wang,[33] X. Wang,[43] X. L. Wang,[38] Y. Wang,[43] J. C. Webb,[45] G. D. Westfall,[25] C. Whitten, Jr.,[6]
H. Wieman,[22] S. W. Wissink,[16] R. Witt,[44] Y. Wu,[50] N. Xu,[22] Q. H. Xu,[22] Y. Xu,[38] Z. Xu,[3] P. Yepes,[36] I-K. Yoo,[34] Q. Yue,[43]
M. Zawisza,[47] H. Zbroszczyk,[47] W. Zhan,[21] H. Zhang,[3] S. Zhang,[39] W. M. Zhang,[19] Y. Zhang,[38] Z. P. Zhang,[38] Y. Zhao,[38]
C. Zhong,[39] J. Zhou,[36] R. Zoulkarneev,[13] Y. Zoulkarneeva,[13] and J. X. Zuo[39]

(STAR Collaboration)

[1]Argonne National Laboratory, Argonne, Illinois 60439, USA
[2]University of Birmingham, Birmingham, United Kingdom
[3]Brookhaven National Laboratory, Upton, New York 11973, USA
[4]University of California, Berkeley, California 94720, USA
[5]University of California, Davis, California 95616, USA
[6]University of California, Los Angeles, California 90095, USA
[7]Universidade Estadual de Campinas, Sao Paulo, Brazil
[8]Carnegie Mellon University, Pittsburgh, Pennsylvania 15213, USA
[9]University of Illinois at Chicago, Chicago, Illinois 60607, USA
[10]Creighton University, Omaha, Nebraska 68178, USA
[11]Nuclear Physics Institute AS CR, 250 68 Řež/Prague, Czech Republic
[12]Laboratory for High Energy (JINR), Dubna, Russia
[13]Particle Physics Laboratory (JINR), Dubna, Russia
[14]Institute of Physics, Bhubaneswar 751005, India
[15]Indian Institute of Technology, Mumbai, India
[16]Indiana University, Bloomington, Indiana 47408, USA
[17]Institut de Recherches Subatomiques, Strasbourg, France
[18]University of Jammu, Jammu 180001, India
[19]Kent State University, Kent, Ohio 44242, USA
[20]University of Kentucky, Lexington, Kentucky, 40506-0055, USA
[21]Institute of Modern Physics, Lanzhou, China
[22]Lawrence Berkeley National Laboratory, Berkeley, California 94720, USA
[23]Massachusetts Institute of Technology, Cambridge, Massachusetts 02139-4307, USA
[24]Max-Planck-Institut für Physik, Munich, Germany
[25]Michigan State University, East Lansing, Michigan 48824, USA
[26]Moscow Engineering Physics Institute, Moscow Russia
[27]City College of New York, New York City, New York 10031, USA
[28]NIKHEF and Utrecht University, Amsterdam, The Netherlands
[29]Ohio State University, Columbus, Ohio 43210, USA
[30]Panjab University, Chandigarh 160014, India
[31]Pennsylvania State University, University Park, Pennsylvania 16802, USA
[32]Institute of High Energy Physics, Protvino, Russia
[33]Purdue University, West Lafayette, Indiana 47907, USA
[34]Pusan National University, Pusan, Republic of Korea
[35]University of Rajasthan, Jaipur 302004, India
[36]Rice University, Houston, Texas 77251, USA
[37]Universidade de Sao Paulo, Sao Paulo, Brazil
[38]University of Science & Technology of China, Hefei 230026, China
[39]Shanghai Institute of Applied Physics, Shanghai 201800, China
[40]SUBATECH, Nantes, France
[41]Texas A&M University, College Station, Texas 77843, USA
[42]University of Texas, Austin, Texas 78712, USA
[43]Tsinghua University, Beijing 100084, China
[44]United States Naval Academy, Annapolis, Maryland 21402, USA
[45]Valparaiso University, Valparaiso, Indiana 46383, USA
[46]Variable Energy Cyclotron Centre, Kolkata 700064, India
[47]Warsaw University of Technology, Warsaw, Poland
[48]University of Washington, Seattle, Washington 98195, USA
[49]Wayne State University, Detroit, Michigan 48201, USA
[50]Institute of Particle Physics, CCNU (HZNU), Wuhan 430079, China
[51]Yale University, New Haven, Connecticut 06520, USA
[52]University of Zagreb, Zagreb, HR-10002, Croatia

Three-particle azimuthal correlation measurements with a high transverse momentum trigger particle are reported for pp, $d + $ Au, and Au $+$ Au collisions at $\sqrt{s_{\mathrm{NN}}} = 200$ GeV by the STAR experiment. Dijet structures are observed in pp, $d +$ Au and peripheral Au $+$ Au collisions. An additional structure is observed in central Au $+$ Au data, signaling conical emission of correlated charged hadrons. The conical emission angle is found to be $\theta = 1.37 \pm 0.02(\mathrm{stat})^{+0.06}_{-0.07}(\mathrm{syst})$, independent of $p_\perp$.

Collisions at BNL's Relativistic Heavy Ion Collider (RHIC) create a hot and dense medium that cannot be described by hadronic degrees of freedom [1]. Evidence of this is provided, in part, by jet-quenching: on the away side of a high transverse momentum ($p_\perp$) trigger particle (in azimuth relative to the trigger particle, $\Delta\phi = \phi - \phi_t \approx \pi$), the correlated yield is strongly suppressed at $p_\perp > 2$ GeV/c [2], while at lower $p_\perp$ the yield is enhanced and the correlated hadrons appear to be partially equilibrated with the bulk medium and are broadly distributed in azimuth [3]. A number of physics mechanisms may account for the data: broadened jets due to large angle gluon radiation [4], deflected jets due to collective radial flow of the bulk [5] or path length dependent energy loss [6], and conical emission due to Čerenkov gluon radiation [7] or Mach-cone shock waves generated by large energy deposition in the hydrodynamic medium [8,9].

Identifying the underlying mechanism is important as it may probe the medium properties such as its speed of sound and equation of state [8,9]. To discriminate between the various mechanisms, we have performed an analysis of three-particle azimuthal correlations between a high $p_\perp$ trigger particle and two lower $p_\perp$ associated particles in $\Delta\phi_i = \phi_i - \phi_t$ ($i = 1$, 2) [10]. We integrate over the pseudorapidity (η) direction because the near- and away-side jets are not correlated in η [3]. Many mechanisms predict that pairs of associated hadrons will be shifted away from $\Delta\phi = \pi$, but will remain close to each other ($\Delta\phi_1 \approx \Delta\phi_2$) [4–6]. In contrast, the Mach-cone or Čerenkov radiation scenarios would result in particle emission on a cone around the away-side jet axis. When projected onto the azimuthal direction, the strongest signal of conical emission would be Jacobian peaks where pairs of correlated hadrons appear with equal probability to be close together or to be far apart and symmetric about π (i.e., $\Delta\phi_1 - \pi \approx \pi - \Delta\phi_2$) [9,11]. The latter feature is specific to conical emission. In this letter, we present evidence for correlated hadron pairs that are symmetrically located about π relative to the trigger particle. The analysis is carried out with trigger and associated particles of $3 < p_\perp < 4$ GeV/c and $1 < p_\perp < 2$ GeV/c, respectively, in pp, $d + $Au, and Au $+$ Au collisions at $\sqrt{s_{NN}} = 200$ GeV.

Details of the STAR (Solenoidal Tracker at RHIC) experiment are described elsewhere [12]. This analysis uses 2×10^6 pp, 6.5×10^6 $d + $Au, and 1.2×10^7 minimum bias (MB) and 1.9×10^7 central trigger Au $+$ Au events taken in 2001–2004. The central trigger data set corresponds to approximately 12% of the total geometric cross section, and will be henceforth referred to as "12% central" collisions. Charged particles are reconstructed with the Time Projection Chamber (TPC) [13], which sits in a uniform 0.5 T magnetic field. The Au $+$ Au data are divided into nine centrality bins according to the charged particle multiplicity in the pseudorapidity region $|\eta| < 0.5$ as in [14]. Similarly the $d + $Au data are divided into three

centrality bins of 0%–10%, 10%–20%, and 20%–100%. The trigger and associated particles are restricted to $|\eta| < 1$. Our results are corrected for the centrality-, $p_\perp$-, and ϕ-dependent reconstruction efficiency for associated particles and the ϕ-dependent efficiency for trigger particles, and are normalized per corrected trigger particle.

Various approaches may be taken to measure three-particle correlations [10,11,15]. This analysis treats the event as composed of two components: one is correlated with the trigger, $\hat{Y}_2$, and the other is background uncorrelated with the trigger except the indirect correlation via anisotropic flow. The correlated particle distribution (two-particle correlation) is thus given by

$$\hat{Y}_2(\Delta\phi) = Y_2(\Delta\phi) - aB_{\text{inc}}F_2(\Delta\phi), \quad (1)$$

where $Y_2(\Delta\phi) = dN/d\Delta\phi$ is the raw associated particle density per trigger. The other, background term is constructed by mixing triggers with different inclusive events (i.e., MB events within a given centrality bin), with the effect of anisotropic flow,

$$F_2(\Delta\phi) = 1 + 2v_2^{(t)}v_2\cos(2\Delta\phi) + 2v_4^{(t)}v_4\cos(4\Delta\phi), \quad (2)$$

constructed pairwise using flow measurements ($v_n^{(t)}$ and v_n, $n = 2$, 4, are trigger and associated particle nth harmonic coefficients, respectively) [16,17]; $B_{\text{inc}} = N_{\text{inc}}/2\pi$ is the inclusive event associated multiplicity density; $a = N_{\text{bg}}/N_{\text{inc}}$ scales N_{inc} to the underlying background associated multiplicity N_{bg} in trigger events, as discussed below.

In our *two-component approach*, the full three-particle distribution, Y_3, consists of the correlated triplets of interest, $\hat{Y}_3$, sets of three particles that are uncorrelated with each other except via flow, and cases where two of the particles are correlated (including jets and other correlations such as resonance decays) and the third is uncorrelated with the first two except via flow. The correlated pair distribution (three-particle correlation) is obtained by [10,11]

$$\hat{Y}_3(\Delta\phi_1, \Delta\phi_2) = Y_3(\Delta\phi_1, \Delta\phi_2) - aB_{\text{inc}}[\hat{Y}_2(\Delta\phi_1)F_2(\Delta\phi_2)$$
$$+ \hat{Y}_2(\Delta\phi_2)F_2(\Delta\phi_1)]$$
$$- ba^2 Y_2^{\text{inc}}(\Delta\phi_1, \Delta\phi_2)$$
$$\times \left[1 + \frac{F_3(\Delta\phi_1, \Delta\phi_2)}{F_2(\Delta\phi_1 - \Delta\phi_2)}\right], \quad (3)$$

where $Y_3 = d^2N/d\Delta\phi_1 d\Delta\phi_2$ is the raw associated particle pair density per trigger, and the second and third terms on the right-hand side are backgrounds. The second term, referred to as *trig-corr-bkgd*, arises from combining a correlated trigger-associated pair with a background particle, and is constructed from the product of the two-particle correlation and its flow-modulated background.

The third term, referred to as *trig-bkgd-bkgd*, arises from combining a trigger with two background particles, and
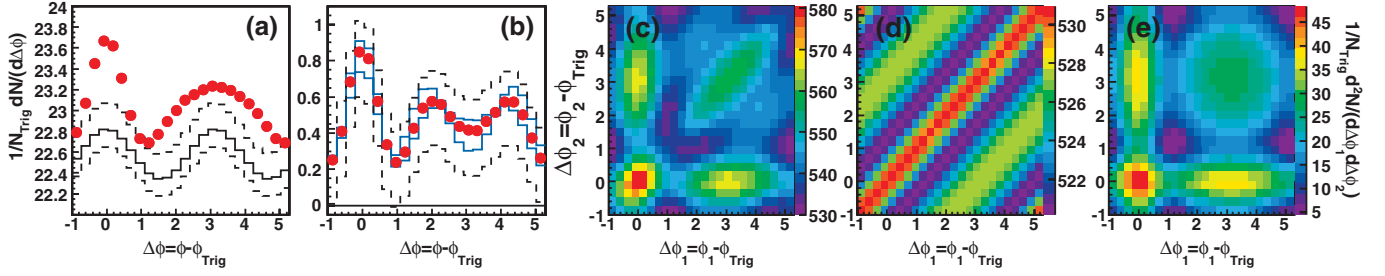
FIG. 1 (color).   (a) Raw two-particle correlation signal Y_2 (red), background $aB_{inc}F_2$ (solid histogram), and background systematic uncertainty from a (dashed histograms). (b) Background-subtracted two-particle correlation $\hat{Y}_2$ (red), and systematic uncertainties due to a (dashed histograms) and flow (blue histograms). (c) Raw three-particle correlation Y_3. (d) $ba^2Y_2^{inc}$. (e) Sum of trig-corr-bkgd and trigger flow. Data are from 12% central Au + Au collisions. Statistical errors in (a),(b) are smaller than the point size.

contains all correlations between the two background particles as well as the flow correlation between them and the trigger. The former is the inclusive event pair density $Y_2^{inc} = d^2N_{inc}/d\Delta\phi_1 d\Delta\phi_2$ relative to a random trigger ϕ_t, which is constructed by mixing the trigger from one event with two particles from another, inclusive event. The latter is referred to as *trigger flow*, where

$$F_3(\Delta\phi_1, \Delta\phi_2) = F_2(\Delta\phi_1) + F_2(\Delta\phi_2) - 2$$
$$+ 2v_2^{(t)}v_2^{(1)}v_4^{(2)}\cos2(\Delta\phi_1 - 2\Delta\phi_2)$$
$$+ 2v_2^{(t)}v_2^{(2)}v_4^{(1)}\cos2(2\Delta\phi_1 - \Delta\phi_2)$$
$$+ 2v_2^{(1)}v_2^{(2)}v_4^{(t)}\cos2(\Delta\phi_1 + \Delta\phi_2) \quad (4)$$

is constructed tripletwise by mixing the trigger with particles from two different inclusive events. The factor ba^2 scales the number of pairs in inclusive events, $\langle N_{inc}(N_{inc} - 1)\rangle$, to that in the underlying background, $\langle N_{bg}(N_{bg} - 1)\rangle$. Non-Poisson multiplicity fluctuations, which can be different in inclusive events and in the background underlying trigger events, result in deviations of b from one. We approximate b by $\frac{\langle N(N-1)\rangle/\langle N\rangle^2}{\langle N_{inc}(N_{inc}-1)\rangle/\langle N_{inc}\rangle^2}$, where N is the associated multiplicity in trigger events.

The analysis procedure is performed and the scaling factors a and b are determined for each centrality bin separately; the final three-particle results are combined over centrality bins to increase the statistics. The value of a is determined assuming that the three-particle correlation

signal has zero yield at minimun (3-ZYAM); the total size of the minimum signal regions is chosen to be 10% of $(2\pi)^2$. It is so chosen so that it is small enough to approximate the real minimum, but large enough to avoid large statistical fluctuations. This size is varied between 5%–15% of $(2\pi)^2$, keeping a fixed, to assess the systematic uncertainty on b. The upper end of the systematic uncertainty on a is taken to be the a value from two-particle ZYA1 (Zero Yield At 1 rad) where $\hat{Y}_2(\Delta\phi)$ vanishes at $|\Delta\phi \pm 1| < \pi/18$ [3]. The lower end is determined, while keeping b at its default value, from the lowest data point (out of total 24×24), which should be lower than the true 3-ZYAM because of statistical fluctuations. With a at each systematic end, the value of b is readjusted, shifting the three-particle correlation result by an approximately constant pedestal, to preserve 3-ZYAM. For the top 5% centrality fraction with the 12% central data, $a = 0.994(^{+0.005}_{-0.004})$ and $b = 1.00021(^{+0.00003}_{-0.00005})$.

Figure 1 shows two-particle correlations in Au + Au central collisions: the raw $Y_2(\Delta\phi)$ and the a-scaled background $aB_{inc}F_2(\Delta\phi)$ in (a), and the background-subtracted $\hat{Y}_2(\Delta\phi)$ in (b). Fitting $\hat{Y}_2(\Delta\phi)$ to various functional forms similar to those in Ref. [18] yields away-side peaks centered 1.18–1.34 rads from π. Figures 1(c)–1(e) show, respectively, the raw three-particle correlation $Y_3(\Delta\phi_1, \Delta\phi_2)$, $ba^2Y_2^{inc}$, and the trig-corr-bkgd term plus trigger flow [19].

Table I summarizes the major sources of systematic uncertainties. (I) Uncertainty in the normalization factor

TABLE I.   Systematic uncertainties on three-particle correlation strength on the away side: central region ($|\Delta\phi_{1,2} - \pi| < 0.35$) and off-diagonal region ($|\Delta\phi_1 - \pi \pm 1.37| < 0.35$ and $|\Delta\phi_2 - \pi \mp 1.37| < 0.35$).

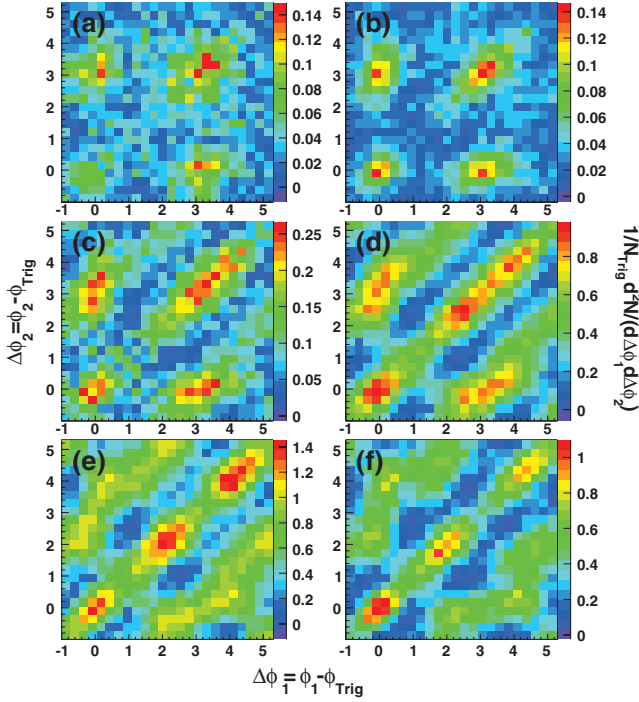| Source	d + Au	$50 - 30\%$ Au + Au		12% central Au + Au	
	cent.	cent.	off-diag.	cent.	off-diag.
(I) a	$^{+16}_{-18}$%	$^{+29}_{-60}$%	$^{+30}_{-63}$%	$^{+42}_{-61}$%	$^{+21}_{-32}$%
(II) v_2	-	$^{-8}_{+17}$%	$^{+36}_{-14}$%	$^{-13}_{+45}$%	$^{+32}_{-16}$%
(III) RP	-	$+11$%	$+8$%	$+32$%	$+5$%
others	$^{+11}_{-10}$%	$^{+12}_{-11}$%	$^{+18}_{-12}$%	$^{+16}_{-20}$%	±12%

FIG. 2 (color). Background-subtracted three-particle correlations, $\hat{Y}_3$, for (a) pp, (b) $d + $ Au, (c) $80 - 50\%$ Au $+$ Au, (d) $50 - 30\%$ Au $+$ Au, (e) $30 - 10\%$ Au $+$ Au, and (f) 12% central Au $+$ Au. Statistical errors per bin are approximately ± 0.012 in (a) and ± 0.006 in (b), both at (π, π), and are ± 0.022, ± 0.049, ± 0.099 and ± 0.077 from (c) to (f), similar for all bins.

a is assessed as above. (II) The v_2 used is the average of modified reaction plane $v_2\{$MRP$\}$ and four-particle cumulant $v_2\{4\}$ [3]. The two-particle cumulant $v_2\{2\}$, which contains flow fluctuations and potentially nonflow effects, and the $v_2\{4\}$ or $v_2\{$2D$\}$ (obtained from a two-dimensional

analysis in $\Delta \eta$ and $\Delta \phi$) bracket the systematic uncertainties. We used a parameterization of $v_4 = 1.15 v_2^2$ [17] and the v_2 uncertainties are propagated. (III) The trig-corr-bkgd term in Eq. (3) is constructed from the two-particle correlation and its background, both averaged over the reaction plane (RP) angle. The effect of the change of the correlation structure with the angle between the trigger and the RP [20] is estimated and included in our final results. The size of the effect is assigned as a single-sided systematic uncertainty. The systematic uncertainty from (I) primarily impacts the overall magnitude of the correlation, with little influence on the shape, whereas those from (II) and (III) have a smaller impact on the magnitude, but affect the shape of the correlation.

Table I also lists the total systematic uncertainty from other, minor sources: uncertainty in the normalization factor b estimated as above; $\pm 20\%$ uncertainty on the unmeasured $v_4^{(t)}$ [17]; uncertainties due to the finite centrality bins on trig-corr-bkgd and trig-bkgd-bkgd terms estimated by breaking each centrality into finer bins; and 10% uncertainty due to the efficiency correction.

Figure 2 shows the background-subtracted three-particle azimuthal correlations, $\hat{Y}_3$, in MB pp, $d + $ Au, and three combined centrality bins of MB Au $+$ Au and the 12% central collisions. Four distinct peaks are observed for each data set, corresponding to both correlated particles on the near side (around $\Delta \phi_1 = \Delta \phi_2 = 0$), both on the away side (around π), and one on each side. The near-side peaks are slightly elongated along the diagonal, probably due to momentum balance in combination with the fact that the trigger direction differs from its parent's.

The away-side central peak is elongated along the diagonal, progressively from pp to $d + $ Au to Au $+$ Au collisions. This indicates that the away-side pairs stay
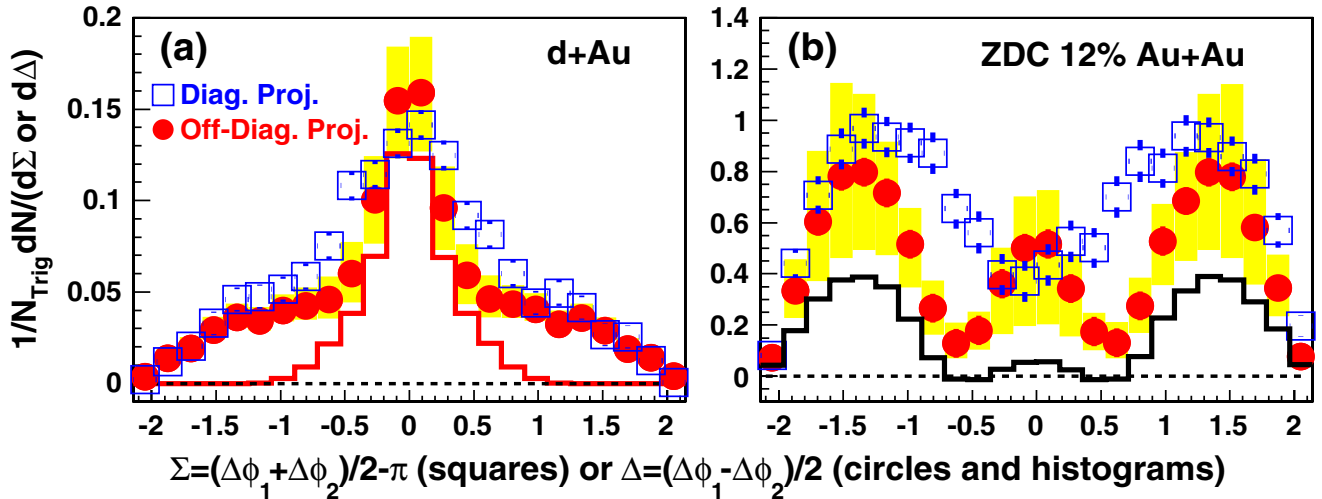

FIG. 3 (color online). Projections of away-side three-particle correlations along the diagonal Σ within $0 < \Delta < 0.35$ (squares) and along the off-diagonal Δ within $|\Sigma| < 0.35$ (points) in (a) $d + $ Au and (b) 12% central Au $+$ Au collisions. The shaded areas indicate systematic uncertainties on the off-diagonal projections. The histogram in (a) is the near-side off-diagonal projection. The histogram in (b) is the away-side off-diagonal projection of our result with $a = b = 1$.
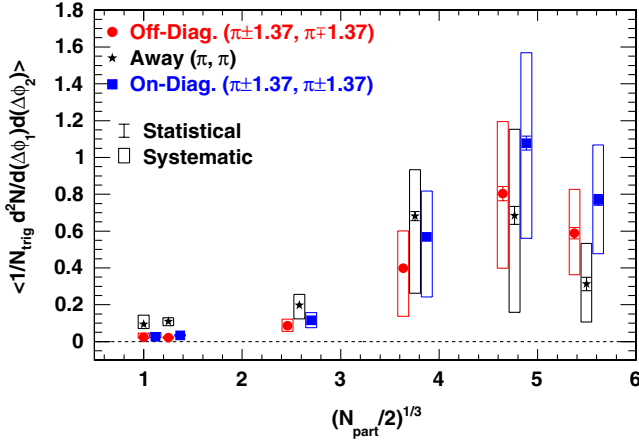
FIG. 4 (color online).   Three-particle correlation strength per
rad^2 versus $(N_{\mathrm{part}}/2)^{1/3}$, where N_{part} is the number of partici-
pants. Some of the data points have been displaced in N_{part} for
clarity.

relatively close while their angles vary over a wide range
event-by-event. Figure 3(a) shows the effect quantitatively
by projecting the d + Au three-particle correlation on the
away side ($1 < \Delta\phi_{1,2} < 2\pi - 1$) along the diagonal in
$\Sigma = (\Delta\phi_1 + \Delta\phi_2)/2 - \pi$ and off-diagonal in $\Delta = (\Delta\phi_1 - \Delta\phi_2)/2$, within the ranges of $0 < \Delta < 0.35$ and
$|\Sigma| < 0.35$, respectively [19]. For comparison the off-
diagonal projection on the near side ($|\Delta\phi_{1,2}| < 1$) is also
shown.

For central Au + Au collisions, additional peaks are
observed in Fig. 2 on the away side along the off-diagonal,
indicating large opening angles between the away-side
correlated pairs, symmetric about π, $\Delta\phi_1 - \pi \approx \pi - \Delta\phi_2$ corresponding to each off-diagonal peak. The
observed correlation pattern in central collisions is quite
different from the expectations for statistical global mo-
mentum conservation [21]. Figure 3(b) shows the diagonal
and off-diagonal projections of the away-side three-
particle correlation result from the 12% central data. The
off-diagonal projection of our result with $a = b = 1$ is also
shown. The off-diagonal side peaks are prominent; these
peaks are evidence of conical emission of charged hadrons
correlated with high $p_\perp$ trigger particles. The side peaks in
the diagonal projection contain conical emission and pos-
sibly other contributions such as $k_\perp$ broadening, large
angle gluon radiation, and deflected jets.

The angular distance θ of the off-diagonal peak loca-
tions from π is obtained by fitting the off-diagonal projec-
tions to a central plus two symmetric side Gaussians. For
12% central Au + Au, $\theta = 1.37 \pm 0.02(\mathrm{stat})^{+0.06}_{-0.07}(\mathrm{syst})$ rad.
The difference between θ and the fit position to two-
particle correlation may arise because the latter mea-
sures a combination of effects. The value of θ does not
depend on centrality or the associated particle $p_\perp$. For
$p_\perp = 0.5$–1,   1–1.5,   1.5–2,   2–3 GeV/c, $\theta = 1.38 \pm$

$0.03(\mathrm{stat})^{+0.07}_{-0.05}(\mathrm{syst})$, $1.36 \pm 0.04^{+0.08}_{-0.07}$, $1.29 \pm 0.04^{+0.19}_{-0.10}$,
and $1.31 \pm 0.05^{+0.25}_{-0.09}$, respectively. If the observed conical
emission is generated by Mach-cone shock waves, the
measured angle θ reflects the speed of sound in the created
medium averaged over the evolution of the collision [8,9].

To characterize the correlation strength, the average
signals are evaluated within 0.7×0.7 rad^2 centered at
$(\Delta\phi_1, \Delta\phi_2) = (\pi, \pi)$, $(\pi \pm 1.37,\ \pi \pm 1.37)$, and $(\pi \pm 1.37,\ \pi \mp 1.37)$. Figure 4 shows the average signal strength
[19] in pp, d + Au, and Au + Au collisions as a function
of $(N_{\mathrm{part}}/2)^{1/3}$. The signal strength increases and appears to
saturate in central collisions. While the away central peak
is the dominant structure in pp, d + Au, and peripheral
Au + Au, the diagonal and off-diagonal side peaks in-
crease rapidly in strength with centrality and become the
dominant structures in central Au + Au collisions.

In conclusion, the first three-particle azimuthal correla-
tion measurements with a high transverse momentum trig-
ger particle are reported by the STAR experiment. The
analysis treats the event as composed of two components,
one correlated with the trigger and the other, background.
Results are presented for minimum bias pp, d + Au, and
different centralities in Au + Au collisions at $\sqrt{s_{\mathrm{NN}}} =$
200 GeV between a trigger particle of $3 < p_\perp < 4$ GeV/c and two associated particles of $1 < p_\perp < 2$ GeV/c. Dijet structures are observed in pp, d + Au
and peripheral Au + Au collisions, with a progressive
diagonal elogation of the away-side central peak. Distinct
peaks at $\theta = 1.37 \pm 0.02(\mathrm{stat})^{+0.06}_{-0.07}(\mathrm{syst})$ from π are ob-
served on the away side in central Au + Au collisions, with
correlated hadron pairs far apart, symmetric about π.
These structures are evidence of conical emission of had-
rons correlated with high $p_\perp$ particles. The conical emis-
sion angle is measured to be independent of the associated
particle $p_\perp$.

[1] J. Adams *et al.*, Nucl. Phys. **A757**, 102 (2005).
[2] C. Adler *et al.*, Phys. Rev. Lett. **90**, 082302 (2003).
[3] J. Adams *et al.*, Phys. Rev. Lett. **95**, 152301 (2005).

[4] I. Vitev, Phys. Lett. B **630**, 78 (2005); A. D. Polosa and C. A. Salgado, Phys. Rev. C **75**, 041901(R) (2007).

[5] N. Armesto, C. A. Salgado, and U. A. Wiedemann, Phys. Rev. Lett. **93**, 242301 (2004).

[6] C. B. Chiu and R. C. Hwa, Phys. Rev. C **74**, 064909 (2006).

[7] I. M. Dremin, Nucl. Phys. **A767**, 233 (2006); V. Koch, A. Majumder, and X.-N. Wang, Phys. Rev. Lett. **96**, 172302 (2006).

[8] H. Stoecker, Nucl. Phys. **A750**, 121 (2005); J. Casalderrey-Solana, E. Shuryak, and D. Teaney, J. Phys. Conf. Ser. **27**, 22 (2005); J. Ruppert and B. Muller, Phys. Lett. B **618**, 123 (2005); A. K. Chaudhuri and U. Heinz, Phys. Rev. Lett. **97**, 062301 (2006); T. Renk and J. Ruppert, Phys. Rev. C **73**, 011901(R) (2006).

[9] T. Renk and J. Ruppert, Phys. Rev. C **76**, 014908 (2007).

[10] Jason G. Ulery, Ph.D. thesis, Purdue University, 2007, arXiv:0801.4904.

[11] J. G. Ulery and F. Wang, Nucl. Instrum. Methods Phys. Res., Sect. A **595**, 502 (2008).

[12] K. H. Ackermann *et al.*, Nucl. Instrum. Methods Phys. Res., Sect. A **499**, 624 (2003).

[13] K. H. Ackermann *et al.*, Nucl. Phys. **A661**, 681 (1999); M. Anderson *et al.*, Nucl. Instrum. Methods Phys. Res., Sect. A **499**, 659 (2003).

[14] J. Adams *et al.*, Phys. Rev. Lett. **92**, 112301 (2004).

[15] C. A. Pruneau, Phys. Rev. C **74**, 064910 (2006).

[16] C. Adler *et al.*, Phys. Rev. C **66**, 034904 (2002).

[17] J. Adams *et al.*, Phys. Rev. C **72**, 014904 (2005).

[18] A. Adare *et al.*, Phys. Rev. C **78**, 014901 (2008).

[19] All three-particle results are symmeterized between $\Delta\phi_1$ and $\Delta\phi_2$. In the off-diagonal projections in Fig. 3 only half the data points are statistically independent; the slight asymmetry in the plots is due to binning. The statistical errors are multiplied by $\sqrt{2}$ in Fig. 4 to account for this.

[20] J. Adams *et al.*, Phys. Rev. Lett. **93**, 252301 (2004).

[21] N. Borghini, Phys. Rev. C **75**, 021904(R) (2007).